# On the Coupling of Ultrasound to $F^{19}$ Nuclear Spins in Antiferromagnetic $RbMnF_3$ †

J. B. Merry*
*Arthur Holly Compton Research Laboratories, Washington University, St. Louis, Missouri* 63130
*and Air Force Cambridge Research Laboratories, Bedford, Massachusetts* 01730

and

Peter A. Fedders and D. I. Bolef
*Arthur Holly Compton Research Laboratories, Washington University, St. Louis, Missouri* 63130
(Received 8 October 1971)

The magnetoelastic theory of the interaction of ultrasound with coupled electronic and nuclear spins in cubic antiferromagnets is used to explain the nuclear-acoustic-resonance (NAR) spectrum of $F^{19}$ in $RbMnF_3$. The coupling mechanism capable of accounting for the proper temperature and angular dependence is found to be forbidden in a perfectly ordered $RbMnF_3$ lattice. With the assumption of a simple model of lattice imperfection, however, the magnitude and anomalous line shape of the observed $F^{19}$ NAR are adequately explained.

## I. INTRODUCTION

The resonant coupling of radio-frequency phonons to the nuclear spins of nonmagnetic ions in antiferromagnetic insulators has been demonstrated by Denison *et al.*[1] and by Mahler and James[2] for $F^{19}$ in $KMnF_3$, and by Melcher *et al.*[3-5] for $F^{19}$ in $RbMnF_3$. Using nuclear-acoustic-resonance (NAR) techniques, Melcher and Bolef[5] examined in detail the $F^{19}$ NAR line shape, temperature dependence, and dependence on magnetic field orientation relative to the direction of propagation $\vec{k}$ of the ultrasound. The $F^{19}$ NAR spectrum observed was intense and unusually complicated compared to that observed for the $F^{19}$ nuclear magnetic resonance.[5-7]

In discussing the angular and temperature dependence of the $F^{19}$ NAR, Melcher and Bolef[5] concluded, with the aid of a phenomenological model, that their results were consistent with a magnetoelastic interaction like that first proposed by Silverstein for uniaxial antiferromagnets.[8,9] Silverstein proposed that the ultrasonic wave gives rise to a time-dependent magnetoelastic interaction which produces a modulation of the effective anisotropy field. This modulation causes a rocking of the sublattice magnetization which in turn couples energy to the nuclei via the hyperfine field.

A magnetoelastic theory has been developed which describes nuclear spin-phonon interactions in a cubic antiferromagnet such as $RbMnF_3$.[10] The predictions of this theory showed excellent agreement with experimental investigations of $Mn^{55}$ NAR in $RbMnF_3$.[11-14] The purpose of the present paper is to show that the magnetoelastic theory also applies to the nuclei of nonmagnetic ions in a cubic antiferromagnet. Application of the magnetoelastic theory gives a result that the coupling mechanism which properly accounts for the observed temperature and angular dependences is forbidden in a perfectly ordered $RbMnF_3$ lattice. This null result is removed, however, in the vicinity of a lattice imperfection.

The theory of $F^{19}$ NMR is reviewed and the derivation of the basic equations of $F^{19}$ NAR is outlined in Sec. II. The theory is compared with experiment in Sec. III; it is found necessary to postulate the existence of lattice imperfections to bring the theory into substantial agreement with experiment. A semiquantitative explanation of the anomalous NAR line shape and magnitude is obtained if one assumes a simple model of a vacancy.

## II. THEORY

Besides the external magnetic field, the resonance frequency of the fluorine nuclei is affected by the magnetic fields due to the manganese ions. The magnetization of these ions couples to the fluorines directly via a dipolar interaction and indirectly via an isotropic Fermi contact interaction.[7] About 98% of this hyperfine field $H_N$ seen by a fluorine nucleus is due to its two nearest Mn neighbors and is given approximately by

$$H_N = \frac{A'}{\gamma_n \hbar} \sum_i \langle S \rangle_i \ .$$

The sum is over nearest neighbors, $A'$ is the hyperfine constant for the coupling between a fluorine nucleus and the electrons of the nearest manganese ion, and $\gamma_n$ is the $F^{19}$ gyromagnetic ratio. In the perfect cubic lattice of $RbMnF_3$, each fluorine has two Mn neighbors with spins oppositely oriented, making $\sum \langle S \rangle_i = 0$ for zero applied field. If $H_0 \neq 0$, the magnetizations no longer cancel exactly and give rise to a small net magnetic moment which is parallel to $\vec{H}_0$. If the magnetizations are in a spin-flopped state (to which case we restrict our discussion in the present paper), they are tilted

by a small angle $t = H_0/2H_E$, where $H_E$ is the exchange field. The effective field seen by the fluorine nuclei is then

$$H_N = \frac{A'\langle S\rangle}{\hbar\gamma_n} 2t = \frac{A'\langle S\rangle H_0}{\hbar\gamma_n H_E} \quad .$$

Because of lattice symmetry, $\vec{H}_N$ is parallel to $\vec{H}_0$. The fluorine nuclei are not at magnetically equivalent sites unless the applied field $H_0 = 0$ or $\vec{H}_0 \| [111]$. If $\vec{H}_0 \| [110]$, there are two nonequivalent sites with a population ratio of 2: 1, resulting in a $F^{19}$ NMR spectrum of two lines. The larger line will be referred to as the 2-F line, the smaller as the 1-F line.

The magnetoelastic nuclear spin-phonon interaction for $F^{19}$ nuclei can be rigorously derived in a manner similar to that for $Mn^{55}$.[10] Again the nuclear spin-phonon interaction proceeds via the electronic (antiferromagnetic) modes. Since there are two electronic modes (termed + and − modes, as in Refs. 10 and 14), there are two NAR modes. For a perfect crystal, we find that the acoustic absorption coefficient due to the two nuclear modes when the system is in a spin-flopped configuration is given by

$$\alpha_\pm = \frac{2\pi Z\gamma_e}{\rho v^2 M_0} \frac{\langle I\rangle \omega_E^2 \omega}{\langle S\rangle \omega_{e\pm}^4} \omega_N^2 B^2 \Gamma_\pm g(\omega) . \qquad (1)$$

In Eq. (1) $\omega_E/\gamma_e$ is the exchange field; $\omega_N/\gamma_n = H_N$ is the hyperfine field; $\omega_{e\pm}$ represent the two nondegenerate antiferromagnetic resonance frequencies; $\langle I\rangle$ and $\langle S\rangle$ are the thermal averages of the $F^{19}$ and electronic spins, respectively; $\gamma_e$ is the electronic gyromagnetic ratio; $\rho$ is the density; $v$ is the acoustic velocity; $M_0$ is the sublattice magnetization; $B$ is the magnetoelastic coupling constant; $\Gamma_\pm$ is a function dependent on the orientation of the external field $\vec{H}_0$ and on the propagation vector $\vec{k}$; $Z$ is the number of fluorine nuclei per unit cell resonating at angular frequency $\omega$; and $g(\omega)$ is a normalized line-shape function. Calculations show that $\alpha_+$ is about five orders of magnitude too small to explain the observed NAR and is characterized by a temperature and angular dependence quite different from that observed.

On the other hand, the expression for $\alpha_-$ contains terms which give a temperature and angular dependence quite similar to that observed. The temperature dependence of the $\alpha_-$ mode is proportional to $(1/T)(BM_0/K)^2$ ($K$ is the anisotropy constant), which agrees with that observed by Melcher and Bolef (see Fig. 5 of Ref. 5). In a perfect crystal, in which each fluorine atom lies equidistant from two Mn ions with oppositely oriented spins, however, the formalism shows that the effects from each Mn ion exactly cancel, giving $\Gamma_- \equiv 0$ and therefore $\alpha_- \equiv 0$. Considering real crystals, the possibility exists that the NAR coupling takes place near sites of crystalline imperfections (vacancies, substitutions, dislocations, etc.) at which the crystalline symmetry is broken. The coefficient multiplying $\Gamma_-$ in the equation for $\alpha_-$ is about 12 orders of magnitude greater than the corresponding coefficient in $\alpha_+$. This fact lends credence to the hypothesis that $F^{19}$ NAR coupling occurs via the relatively few $F^{19}$ nuclei located near lattice imperfections. To explore this possibility, it is convenient to examine the problem in terms of effective crystalline fields, as in Ref. 14. There it was shown that the NAR coupling to the nuclear mode $\omega_{n-}$ ($\omega_{n+}$) proceeds via its corresponding electronic mode $\omega_{e-}$($\omega_{e+}$). The ultrasonically produced magnetoelastic field causes a rocking of the electronic magnetization which modulates the hyperfine field $H_N$. This process stimulates nuclear spin transitions if there is a component of the time-dependent hyperfine field perpendicular to $I_z$. The equilibrium configuration of the internal fields is shown in Fig. 1.

In the spin-flopped case, the electronic (+) mode is excited by rocking the sublattice magnetization in the plane of Fig. 1. The time-dependent field perpendicular to $I_z$ is $H_N \tan\beta$, where $\beta$ is the rocking angle. The electronic (−) mode, on the other hand, is excited by rocking the sublattice magnetization about $\vec{H}_0$. This causes no rocking of the field $\vec{H}_N$ seen by the vast majority of the fluorine nuclei, since $\vec{H}_N \| \vec{H}_0$ for these nuclei. The fields are collinear because of lattice symmetry; the fluorine nuclei are located equidistantly between two Mn ions with oppositely oriented magnetic moments. For fluorine nuclei near sites of crystalline imperfections, these conditions no longer hold and, in general, an electronic dipolar or hyperfine field perpendicular to $\vec{H}_0$ exists. We refer to this field as $H_{N\perp}$. Since only the nonsymmetrically located $F^{19}$ nuclei contribute to the NAR spectrum, $H_N^2$ in Eq. (1) for the (−) mode should be replaced by

$$(H_N')^2 = \frac{1}{N}\sum_i^N |H_{N\perp}(i)|^2 , \qquad (2)$$

where $N$ is the number of unit cells in the crystal and the sum is over one particular fluorine site per unit cell. With this modification, $\alpha_-$ is no longer identically zero.

## III. COMPARISON WITH EXPERIMENT

We attempt to show in this section that the impor-

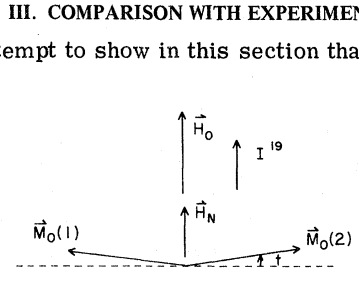


FIG. 1. Equilibrium configuration of the internal fields of $RbMnF_3$.

TABLE I. Comparison of calculated and observed $F^{19}$ NAR angular dependencies. [The NAR absorption ($\alpha$) is in Hz.]

| Case number | Configuration | $B_-^2\Gamma_-$ | (1) $\psi$ | (2) $B$ | (3) $\Gamma_-$ | (4) $\Gamma_s$ | (5) $\alpha(\Gamma_-)$ | (6) $\alpha(\Gamma_s)$ | (7) $\alpha_{obs}$ |
|---|---|---|---|---|---|---|---|---|---|
| 1 | $\vec{k}_l \parallel [011]$, $\vec{H}_0$ in (100) | $\frac{(b_1-b_2\sin^2 2\psi)^2\ 2(2-\sin^2 2\psi)}{(4-\sin^2 2\psi)^2}$ | 0, 90 | $b_1$ | 0.25 | 0.25 | 43 | 43 | 37 |
| 2 | | | 45 | $b_1-b_2$ | 0.22 | 0.22 | 12 | 12 | 14 |
| 3 | | | 135 | $b_1+b_2$ | 0.22 | 0.22 | 15 | 15 | 17 |
| 4 | $\vec{k}_s \parallel [001]$, $\hat{e} \parallel [100]$, $\vec{H}_0$ in (100) | $\frac{b_2^2\cos^4\psi\sin^6\psi}{(4-\sin^2 2\psi)^2}$ | 0 | | 0 | 0 | 0 | 0 | $\leq 0.07$ |
| 5 | | | 45 | $b_2$ | 0.05 | 0.50 | 0.01 | 0.18 | 0.16 |
| 6 | | | 90 | $b_2$ | 0 | 0.10 | 0 | 0.99 | 0.77 |

tant characteristics of the observed $F^{19}$ NAR spectrum can indeed be accounted for on the basis of the magnetoelastic interaction via the (–) mode. To obtain agreement between the theoretically predicted and the observed spectrum it is necessary to postulate a deviation of $\vec{M}_0$ from the usual equilibrium orientation. We discuss in turn (i) the NAR angular dependence, and (ii) the NAR line intensity and line shape.

### A. NAR Angular Dependence

The angular factors $B_-^2\Gamma_-$ of Eq. (1) corresponding to two configurations of $\vec{H}_0$ and $\vec{k}$ are given in Table I. In this table $b_1$ and $b_2$ are the magnetoelastic constants for, respectively, the longitudinal and transverse waves, and $\psi$ is the angle that $\vec{H}_0$ makes with the $z$ axis [001]. The values of the NAR attenuation $\alpha(\Gamma_-)$ calculated[13] using these values of $B_-^2\Gamma_-$ are given in column 5. The agreement between $\alpha(\Gamma_-)$ and the experimentally observed NAR attenuation $\alpha_{obs}$ is seen to be good for four of the six cases shown. In seven other cases calculated in a similar manner (not shown in Table I), agreement was also good.[13] For the last two cases shown in Table I, $\alpha(\Gamma_-)$ is much smaller than $\alpha_{obs}$. We believe that the origin of the discrepancy lies in the assumption of the equilibrium orientation of $\vec{M}_0$. For the calculation of the angular factor $\Gamma$, it is essential to know this orientation. Thus far it has been assumed that the anisotropy field $\vec{H}_A$ lies along the [111] or easy axes and that the [100] are the hard axes. In that case the flopped spins, which lie in a plane perpendicular to $\vec{H}_0$, assume an easy orientation in that plane. We term this orientation the easy orientation of $\vec{M}_0$. There are several reasons, however, for expecting the orientation of $\vec{H}_A$ to be different than that thus far assumed. The anisotropy field (which determines the easy and hard directions) at 77 K is calculated to be quite small ($\simeq 10^{-3}$ Oe).[15,16] As mentioned above, the fluorine NAR magnetoelastic coupling is expected to be large near sites of crystalline imperfections. At such sites, given the low value of $\vec{H}_A$, the local anisotropy field can be expected to vary in both direction and magnitude, with the result that $\vec{M}_0$ may take any position between the easy and hard orientations.

The explicit equation for $\Gamma_-$ for rows 4–6 of Table I is [13,14]

$$\Gamma_- = \frac{1}{M_0^4}\left[M_z(M_y\cos\psi - M_z\sin\psi) + M_x^2\sin\psi\right]^2. \tag{3}$$

For $\psi = 90°$, $\Gamma_- = (M_x^2 - M_z^2)/M_0^4$. If $\vec{M}_0$ is in an easy configuration, $M_x = M_z = M_0/\sqrt{2}$ and $\Gamma_- = 0$. On the other hand, if $\vec{M}_0$ is parallel to a hard axis, $\Gamma_- = 1$. When $\vec{M}_0$ is parallel to only the hard axes, however, $\Gamma_- = 0$ for all cases other than rows 4–6 of Table I. If we assume that the effective angular factor is made up of contributions with $\vec{M}_0$ in *both* the easy and the hard orientations, we obtain results more consistent with the data. We therefore introduce a new angular factor $\Gamma_s$ which is taken to be the sum of two values of $\Gamma_-$, one calculated for $\vec{M}_0$ in the hard orientation and the other for $\vec{M}_0$ in the easy orientation, i.e., $\Gamma_s = \Gamma_-(\text{easy}) + \Gamma_-(\text{hard})$. The NAR attenuation calculated using $\Gamma_s$ is shown in column 6 of Table I. There is now good over-all agreement between $\alpha(\Gamma_s)$ and $\alpha_{obs}$ for all of the 13 cases which have been calculated,[13] six of which are shown in Table I.

### B. NAR Line Intensity and Line Shape

It remains to be shown that the magnitude and peculiar line shape of the observed $F^{19}$ NAR spectrum[5] can be accounted for by the (–) mode of the magnetoelastic interaction. As discussed above, if this NAR mechanism is to be operative, certain fluorine nuclei must "see" a magnetic moment perpendicular to $\vec{H}_0$. This condition obtains only where the lattice symmetry of $RbMnF_3$ is broken by lattice imperfections. In this section, a model of a particular type of lattice imperfection is proposed and is utilized in calculating the magnitude and line shape of the resulting $F^{19}$ NAR.

A simple type of lattice imperfection which can be shown to give rise to many of the observed effects is a manganese vacancy. For every missing Mn ion there is an uncompensated magnetic moment in the crystal, which produces a dipolar field cen-

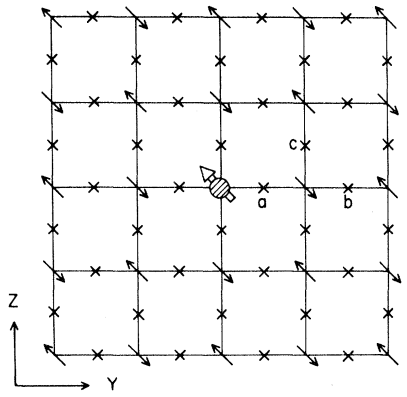


FIG. 2. Diagrammatic sketch of the $y$-$z$ plane of the $RbMnF_3$ lattice with a manganese vacancy. $x$ denotes a $F^{19}$ site, ↑, a $Mn^{55}$ site, and ⊘ a vacancy.

tered at the vacancy site. We shall assume here that this is the only effect of the vacancy. A model of this lattice vacancy is shown schematically in Fig. 2. In this figure, the magnetizations lie in the $y$-$z$ plane and $\vec{H}_0$ is parallel to the $x$ axis. The six fluorines which are nearest to the vacancy (in sites like "a") see a large hyperfine field of ~100 kOe due to an unbalanced pair of sublattice magnetizations. These fluorines are pushed into the uhf region (~400 MHz for 100 kOe) and do not contribute to the observed[5] 10–30-MHz spectrum. The hyperfine field seen by the next-nearest neighbors is insignificant compared to the dipolar field resulting from the vacancy. This field is given by $\vec{B}(r) = [3(\vec{r}\cdot\vec{\mu})\vec{r}/\vec{r}^5 - \vec{\mu}/\vec{r}^3]$, where $\vec{r}$ is centered on the vacancy site, $\mu$ is the dipolar moment of the Mn ion, and $\vec{\mu}$ is parallel to $\vec{M}_0$. The magnitude of the dipolar field seen by the next-nearest fluorine 6.33 Å away from the vacancy is $\mu/(6.33\ \text{Å})^3$ or $514(\langle S\rangle/S_0)$ Oe. The component of $\vec{B}$ parallel to $\vec{H}_0$, $B_\parallel$, causes a shift in the nuclear resonance frequency. The component perpendicular to $\vec{H}_0$, $B_\perp$, corresponds to $H_N'$ in Eq. (2). The fields seen by the next-nearest neighbor (site c shown in Fig. 2) are $B_\perp = 396$ Oe and $B_\parallel = 276$ Oe for $T = 77$ K.

An application of this model is shown in Fig. 3 for the case corresponding to row 5 in Table I. In Fig. 3(a) is shown the unperturbed $F^{19}$ nuclear resonance spectrum (i.e., expected NMR spectrum) for $H_0 = 7$ kOe, $\vec{H} \parallel [110]$, and $T = 77$K. The dashed and solid lines in Fig. 3(a) correspond, respectively, to the 1-F and 2-F lines. The predicted NAR spectrum corresponding to $\Gamma_-$ is shown in Fig. 3(b). We see that the dipolar field has completely dispersed both the 1-F and 2-F lines. In the light of the discussion regarding the orientation of $\vec{M}_0$, the predicted spectrum should be calculated by averaging over-all possible orientations of $\vec{M}_0$. Considering the simplicity of the present model, we choose to approximate this averaging procedure by merely taking the sum of $\alpha$(hard axis) and $\alpha$(easy axis), corresponding to the weighting factor $\Gamma_s$. When the predicted NAR spectrum for $\vec{M}_0$ along a hard axis is added to that of Fig. 3(b), the $\alpha(\Gamma_s)$ spectrum of Fig. 3(c) is obtained. The $F^{19}$ NAR spectrum observed by Melcher and Bolef under conditions corresponding to those assumed in Fig. 3 is shown in Fig. 4. In Fig. 4(a) is shown the recorder tracing of the spectrum which is the derivative of the NAR absorption. In Fig. 4(b) is shown the curve obtained after integrating the curve of Fig. 4(a). The spectra of Figs. 4(b) and 3(c) show many similarities, demonstrating that it is reasonable to assume that lattice imperfections should result in additional broad structure in the vicinity of the perturbed $F^{19}$ lines. There is little similarity, on the other hand, between the spectra of Figs. 4(b) and 3(b). This may be taken as a further indication that $\vec{M}_0$ is not always in an easy configuration.

The temperature dependence of the complicated $F^{19}$ NAR spectrum[3,6] can be explained qualitatively on the basis of the magnetoelastic coupling mechanism. The magnitude of the dipolar field discussed

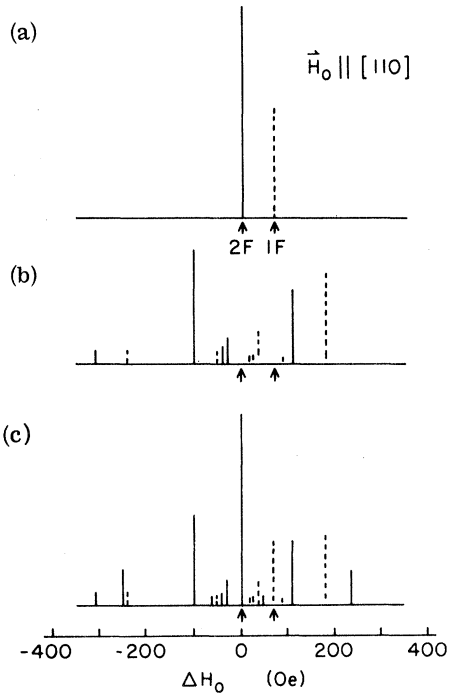


FIG. 3. Calculated $F^{19}$ nuclear resonance spectrum for $T = 77.4$ K and $\vec{H}_0 \parallel [110]$. $\Delta H_0 = 0$ corresponds to $H_0 = 7.0$ kOe: (a) the "unperturbed" or NMR spectrum; (b) the NAR spectrum corresponding to $\alpha(\Gamma_-)$; (c) the NAR spectrum corresponding to $\alpha(\Gamma_s)$. The vertical scale in (c) is twice that in (a) and (b). The arrows indicate expected positions of the unperturbed 1-F and 2-F lines.

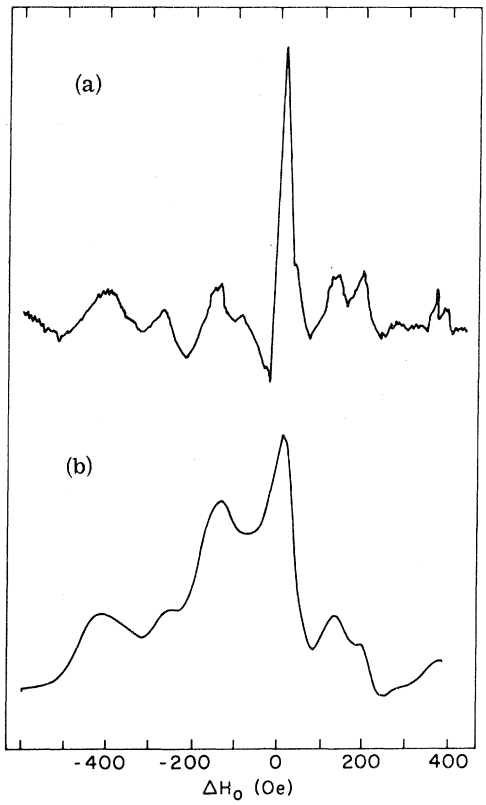


FIG. 4. Flourine NAR spectrum observed by Melcher and Bolef for $H_0 = 7$ kOe, $\vec{H}_0 \| [110]$, $\vec{k}_l \| [110]$, and $T = 77.4$ K: (a) recorder tracing of derivative spectrum; (b) integrated (absorption) spectrum.

above is proportional to $\langle S \rangle$, which is strongly temperature dependent near the Néel point. The fields $B_\parallel$ and $B_\perp$ can be expected to exhibit the same temperature dependence. As the temperature is lowered, $\langle S \rangle$ as well as $B_\parallel$ increases, causing increased line shifting. The magnitude of the shifted lines is also predicted to increase, corresponding to the increase in $B_\perp$. As $T$ is lowered, therefore, the magnitude of the shifted lines grows in relation to that of the unshifted lines. This is the type of temperature dependence observed by Melcher *et al.*[3,6]

We consider, finally, the question of whether a reasonable density of lattice imperfections can account for the magnitude of the observed $F^{19}$ NAR. From Eqs. (1) and (2), one can show that $\alpha_-$ is given by[13]

$$\alpha_- = \frac{1.28 \times 10^{-5} (H_N')^2}{(H_A')^2} \quad , \tag{4}$$

where $H_A' [\simeq \frac{3}{2} B(\psi) H_A]$ is the projection of $\vec{H}_A$ on the sublattice magnetization. [The factor $(\omega_{e-}/\gamma_e)^2$ in Eq. (1) has been written as $(\omega_{e-}/\gamma_e)^2 = 3B(\psi) H_E H_A = 2 H_E H_A'$.] We calculate $\alpha_-$ for the following conditions: longitudinal waves propagated along the [001] axis, $H_0 = 7$ kOe, $\vec{H}_0 \| [100]$, $T = 77$K, $Z = 2$, and $\Gamma_- = 1$. Melcher and Bolef measured the NAR attenuation at the center of the large unshifted line for the conditions stated above and found that $\alpha_- = 180$ Hz.[5] Recalling that $H_A \simeq 10^{-3}$ Oe at 77 K and assuming that all unit cells participate equally in the interaction, Eq. (4) gives $(H_N')^2 \simeq 14$ Oe$^2$. Since only $n$ unit cells with a vacancy are participating in the NAR interaction, $(H_N')^2 = (n/N) \sum |B_\perp(i)|^2$, in which the sum includes all fluorines which are neighbors of a Mn vacancy and which contribute to the 2-F line. Calculations show that $\sum |B_\perp(i)|^2 \simeq 2 \times 10^6$ Oe$^2$ for each Mn vacancy. The fraction of unit cells that must have a vacancy to give the observed intensity is therefore given by $n/N = (H_N')^2 / \sum |B_\perp(i)|^2 \simeq 7 \times 10^{-5}$. Considering that the impurity density in this sample is of the order of $10^{-4}$ (see Ref. 17), this is a reasonable order of magnitude.

Our aim in the preceding discussion and calculation was to substantiate the hypothesis that the magnetoelastic NAR interaction occurs via lattice imperfections. The specific model of lattice imperfection assumed is not critical; other types of imperfections are capable of giving rise to a dipolar field of magnitude sufficient to account for the observed NAR. In particular, a single lattice imperfection undoubtedly affects the magnetization at neighboring sites. Thus a far smaller concentration of defects than assumed above may account for the observed NAR spectrum.

ACKNOWLEDGMENT

We wish to thank J. G. Miller for many helpful discussions and for a critical review of the manuscript.

†Sponsored in part by the National Science Foundation and by the Air Force Office of Scientific Research (PAF) under Grant No. AFOSR-71-2004.

*Presently a NAS-NRC Research Associate at Air Force Cambridge Research Laboratories, Bedford, Mass. 01730.

[1]A. B. Denison, L. W. James, J. D. Currin, W. H. Tantilla, and R. J. Mahler, Phys. Rev. Letters 12, 244 (1964).

[2]R. J. Mahler and L. W. James, J. Appl. Phys. 41, 1633 (1970).

[3]R. L. Melcher, D. I. Bolef, and R. W. H. Stevenson, Phys. Rev. Letters 20, 453 (1968).

[4]R. L. Melcher and D. I. Bolef, Phys. Rev. Letters 20, 1338 (1968).

[5]R. L. Melcher and D. I. Bolef, Phys. Rev. 184, 556 (1969).

[6]R. L. Melcher, Ph. D. thesis (Washington University, St. Louis, Mo., 1968) (unpublished).

[7]M. B. Walker and R. W. H. Stevenson, Proc. Phys. Soc. (London) 87, 35 (1966).

[8]S. D. Silverstein, Phys. Rev. 132, 997(1963).

[9]R. L. Melcher, Phys. Rev. B 1, 4493 (1970).
[10]P. A. Fedders, Phys. Rev. B 1, 3756 (1970).
[11]J. B. Merry and D. I. Bolef, Phys. Rev. Letters 23, 126 (1969).
[12]J. B. Merry and D. I. Bolef, J. Appl. Phys. 41, 1412 (1970).
[13]J. B. Merry, Ph. D. thesis (Washington University, St. Louis, Mo., 1970) (unpublished).
[14]J. B. Merry and D. I. Bolef, Phys. Rev. B 4, 1572 (1971).
[15]M. J. Freiser, R. J. Joenk, P. E. Seiden, and D. T. Teaney, in *Proceedings of the International Conference on Magnetism, Nottingham*, 1964 (The Institute of Physics and the Physical Society, London, 1965).
[16]W. J. Ince, Ph. D. thesis (M. I. T., Cambridge, Mass., 1969) (unpublished).
[17]R. L. Melcher and D. I. Bolef, Phys. Rev. 178, 864 (1969).